Fachtagung "Experimentelle Strömungsmechanik"
4. – 6. September 2018, Rostock

Spektroskopische Analyse von Präkursoren für die Flammensprühpyrolyse

Screening Study on precursor for the Flame Spray Pyrolysis Process

Malte F.B. Stodt[1, 2], Sabine Wagenfeld[2], Udo Fritsching[1, 3], Johannes Kiefer[2]
[1] Leibniz-Institut für Werkstofforientierte Technologien – IWT, Badgasteiner Str. 3, 28359 Bremen
[2] Technische Thermodynamik, Universität Bremen, Badgasteiner Str. 1, 28359 Bremen
[3] Mechanische Verfahrenstechnik, Produktionstechnik, Universität Bremen, Bibliothekstraße 1, 28359 Bremen

IR Spektroskopie, Präkursorchemie, Eisen(III) Nitrat, Eisenoxid, Flammensprühpyrolyse
IR spectroscopy, precursor chemistry, iron(III) nitrate, iron oxide, flame spray pyrolysis

Abstract

Various iron(III) nitrate nonahydrate and *n*-alkyl alcohol solutions have been analyzed using infrared spectroscopy with the purpose of gaining an insight in the precursor chemistry. The effect of chemical reactions occurring within the precursor mixture is supposed to have an impact on the atomization and droplet evaporation within the flame spray pyrolysis process. Moreover, a precipitation mechanism is presented to explain the presence of muddy turbidities in the precursor/solvent mixtures.

Introduction

Nanoparticulate metal oxides are widely used for numerous engineering applications such as energy storage materials, catalysts, polishing slurries or biomedical applications like drug delivery and cellular labeling. Due to the growing demand of such nano-sized metalloxides, there have been tremendous efforts on investigating appropriate production routes for the nanoparticle synthesis using different techniques such as sol-gel reactions, coprecipitation, and polyol methods. However, these routes are rather expensive and require time consuming post processing to obtain highly pure crystalline nanopowders. The flame spray pyrolysis (FSP) is capable of producing metalloxide nanoparticles fast and economically with production rates up to 1.1 kg/h for SiO_2 (Mueller, Mädler, & Pratsinis, 2003) at an industrial scale.

In terms of material diversity, the FSP process is a rather new but already well developed process where many elements of the periodic table can be turned into metal oxides in laboratory scale reactors with production rates of a few grams per hour (Mädler, Kammler, Mueller, & Pratsinis, 2002). Figure 1 shows a schematic drawing of the FSP process using a new air assisted SpraySyn burner developed within the priority program SPP 1980 of the Deutsche Forschungsgemeinschaft (DFG). In this reactor, the combustible solvent (e.g. ethanol) and metallic precursor (e.g. titanium isopropoxide) running from the capillary tube disintegrates into a dense spray (mass median diameter ≈ 10 µm) using a dispersion gas (O_2 or O_2/N_2) for atomization. A concentrically arranged flamelet feeds a stoichiometric mixture of CH_4 and O_2 into the reactor in order to maintain a continuous combustion. A co-flow is implemented for further stabilization and for enclosed operations. Then, along the axial trajectory, the process

Karlsruhe, Germany, ISBN 978-3-9816764-5-7

steps are divided into droplet evaporation, droplet burning, nucleation, particle growth (coalescence, coagulation) and finally agglomeration (Wang, Friedlander, & Mädler, 2005). Depending on the choice of the solvent, the combustion causes an intense release of thermal energy giving rise to flame temperatures of $T > 2000$ K (Gröhn, Pratsinis, & Wegner, 2012).

The choice of a suitable solvent and precursor combination determines the nano-sized metalloxide product in terms of density ρ and viscosity η of the fluid to be atomized, particle size distribution, morphology and purity of particulate phase. However, unwanted chemical reactions including precipitation between precursor and solvent prior to the actual flame spray process may have negative effects such as precipitation (Meierhofer et al., 2017). Besides that, the choice of solvent and precursor combination is challenging since the amount of potential organometallic precursors and solvents on the market is huge within a large price range.

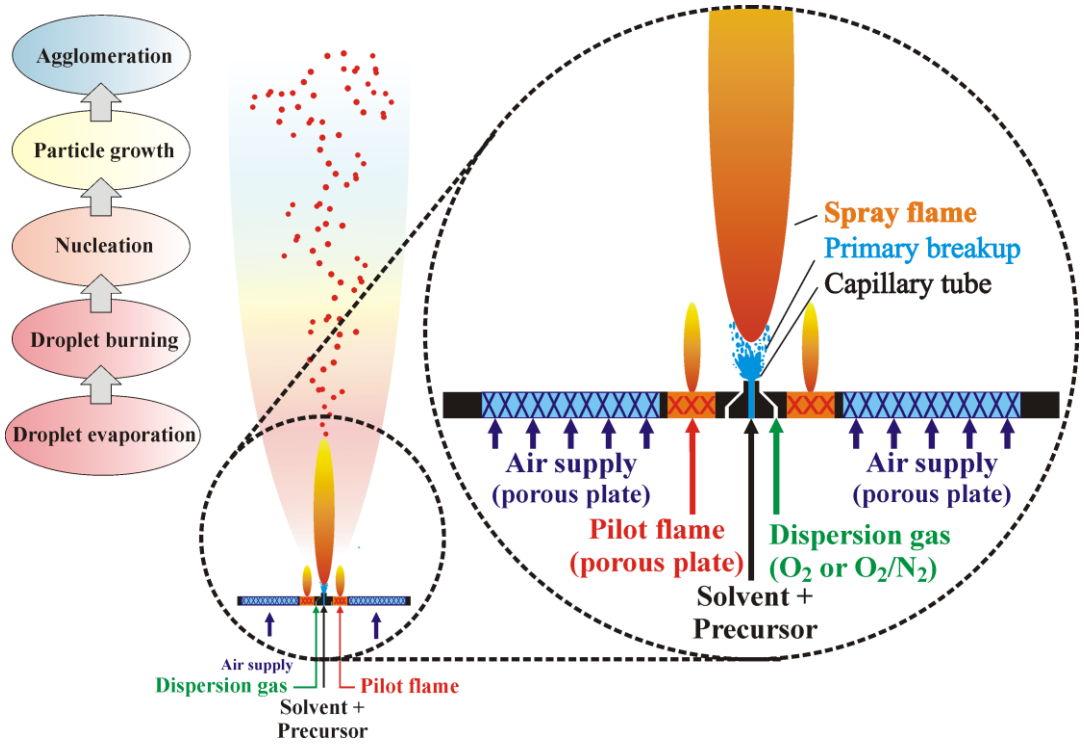

Figure 1: Schematic of flame spray generated by air assisted SpraySyn burner. The liquid jet disintegrates into a dense spray and is ignited by a concentrically arranged premixed pilot flame. The spray combustion mode is dominated by the heat of combustion of the fuel, liquid to gas (L/G) ratio and the chemical reaction rate of the nucleation within the process.

The relevant literature reveals that the efforts in a systematic investigation into the underlying precursor chemistry for mixtures of organic solvents and metal precursors are very limited. Most studies are focused on the analysis of the individual metalloxides but do not take effects of unwanted chemical reactions in the precursor/solvent mixture into account.

In the present study, we aim at gaining an insight into the precursor chemistry, which can have an impact on atomization and particle synthesis. For this purpose, a vibrational study on iron(III) nitrate nonahydrate ($Fe(NO_3)_3 + 9H_2O$) and *n*-alkyl alcohol (n = 2, 3, 4) mixtures within a composition range of 0.01 mol kg^{-1} < b < 1.0 mol kg^{-1}, with b defined as the molality is performed.

The experimental infrared (IR) spectra of the pure compounds and the mixtures are presented and analyzed.

Materials and Methods

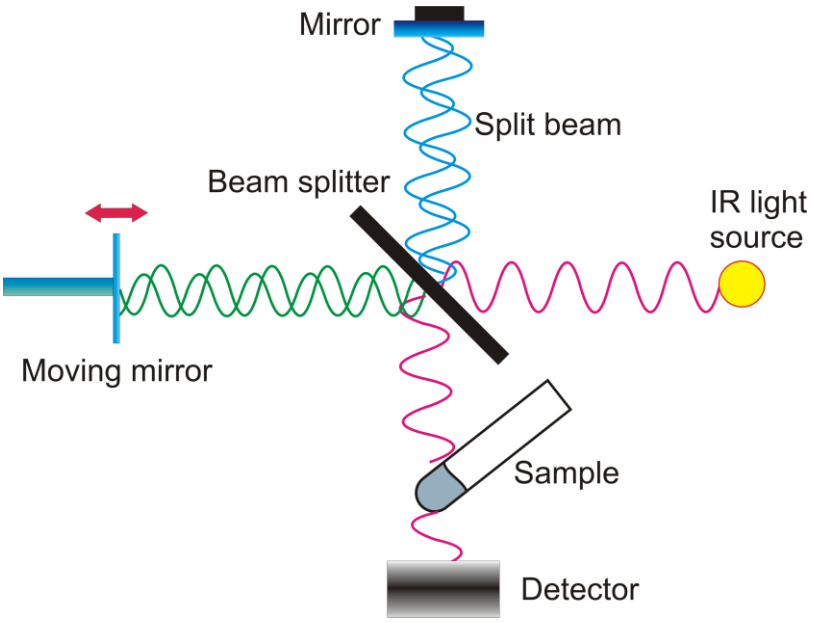

Figure 2: Schematic of a Fourier-transformed infrared spectrometer

All chemicals were used without any further purification with a purity of > 99.5 %. The iron(III) nitrate nonahydrate ($Fe_3(NO_3)_3$ + 9 H_2O) was purchased from Merck (Lot: K48589083712, Merck kGaA, Darmstadt, Germany). As solvents, ethanol (ethanol absolute, Lot: 176124009, VWR Chemicals, Radnor, USA), 1-propanol (Lot: SZBA2670, Sigma-Aldrich, St. Louis, USA), 2-propanol (analytical reagent grade, Lot: 1724392, Fisher Scientific UK ltd., Loughborough, UK), and 1-butanol (analysis number: 337328/1 494, Fluka Chemika, Neu-Ulm, Germany) were used. Before preparing the solutions, the water content of the alcohols was determined by Karl-Fischer titration: w_{H2O} < 508 ppm (ethanol), w_{H2O} < 119 ppm (1-propanol), w_{H2O} < 405 ppm (2-propanol), and w_{H2O} < 430 ppm (1-butanol). The water content of iron(III) nitrate nonahydrate was not determined due to its crystalline structure and its hydration.

The solutions of iron(III) nitrate nonahydrate and alcohols were prepared gravimetrically using an analytical balance. A vortexer is used to dissolve the solid iron(III) nitrate nonahydrate in the solvent until complete dissolution of the crystals of hydrated iron(III) nitrate.
The IR spectra were recorded directly after sample preparation on an Agilent Cary 630 infrared spectrometer with a ZnSe ATR module at room temperature (T = 293 K) and ambient pressure (p = 1 atm). Figure 2 shows the working principle of the interferometer. The spectra were recorded within a range from 650 cm^{-1} to 4000 cm^{-1} at a nominal resolution of 2 cm^{-1}. In order to avoid measurement errors due to solvent evaporation during the measurement, 8 scans were recorded and averaged.

Results and discussion

In this section, an overview of the vibrational spectra and a detailed discussion on characteristic peak regions are given.

Solubility

The solubility of iron(III) nitrate in *n*-alkyl alcohols (*n* = 2, 3, 4) has not been reported in the literature yet. Therefore, no solvation limits as function of temperature *T* are known. Nevertheless, the time required to dissolve iron(III) nitrate in the primary *n*-alkyl alcohols was found to decrease with increasing alkyl chain length, owing to the stronger hydrogen bond strength of the alcohols. When dissolving iron(III) nitrate nonahydrate in 2-propanol significant precipitation was observed. A deeper description will be provided in the section *Precipitation.*

Screening studies

Figure 3 displays the IR spectra of neat ethanol and iron(III) nitrate nonahydrate and their mixtures. The IR spectra are normalized with respect to their strongest signal peak, which is a sharp CO stretching mode (1040 – 1052 cm^{-1}) for all the alcohols and a broad antisymmetric NO_3 peak (1364 cm^{-1}) for the iron(III) nitrate nonahydrate.

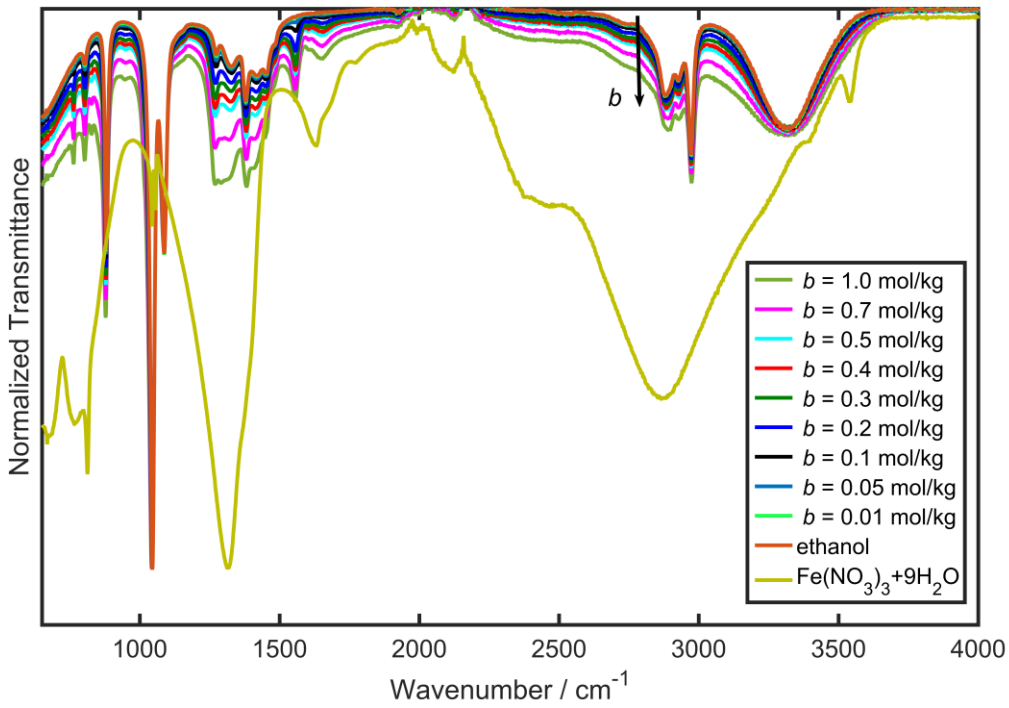

Figure 3: Infrared spectra of pure ethanol and iron(III) nitrate nonahydrate and their mixtures.

The IR spectra of the normal alkyl alcohols have already been described in the literature and the effect of the chain length on the vibrational structure are well understood (Kiefer, Wagenfeld, & Kerlé, 2018). Therefore, only a short overview of characteristic vibration modes is given. In Figure 4 the IR spectra of the underlying iron(III) nitrate nonahydrate and alcohol mixtures and their respective neat solvents are shown. Between 3100 and 3650 cm^{-1}, the characteristic broad band of the OH group stretching vibrations can be seen. This broad band is frequently used as a marker for intermolecular interactions (Kiefer et al., 2018; Paolantoni, Sassi, Morresi, & Cataliotti, 2005; Sassi, Morresi, Paolantoni, & Cataliotti, 2002; Zheng, Sun, & Shi, 2011) since it can act as donor and acceptor for hydrogen bonds.

Karlsruhe, Germany, ISBN 978-3-9816764-5-7

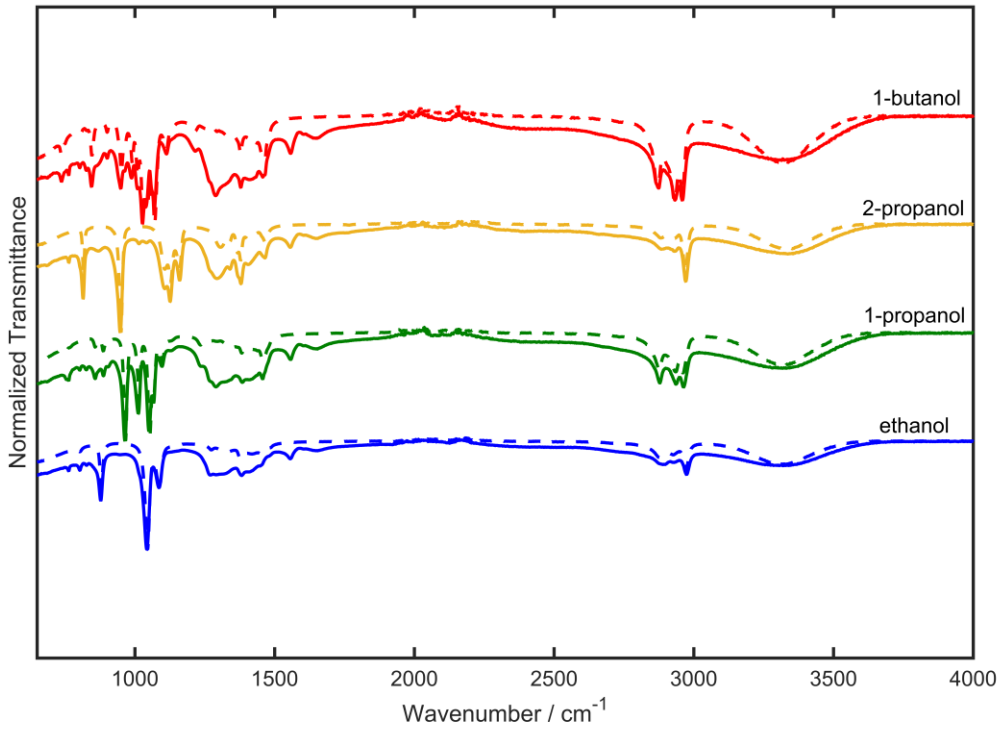

Figure 4: Dashed lines display IR spectra of neat alcohols. The solid lines represent IR spectra of $Fe(NO_3)_3\ 9H_2O$ and alcohol mixtures for b = 1.0 mol kg^{-1}.

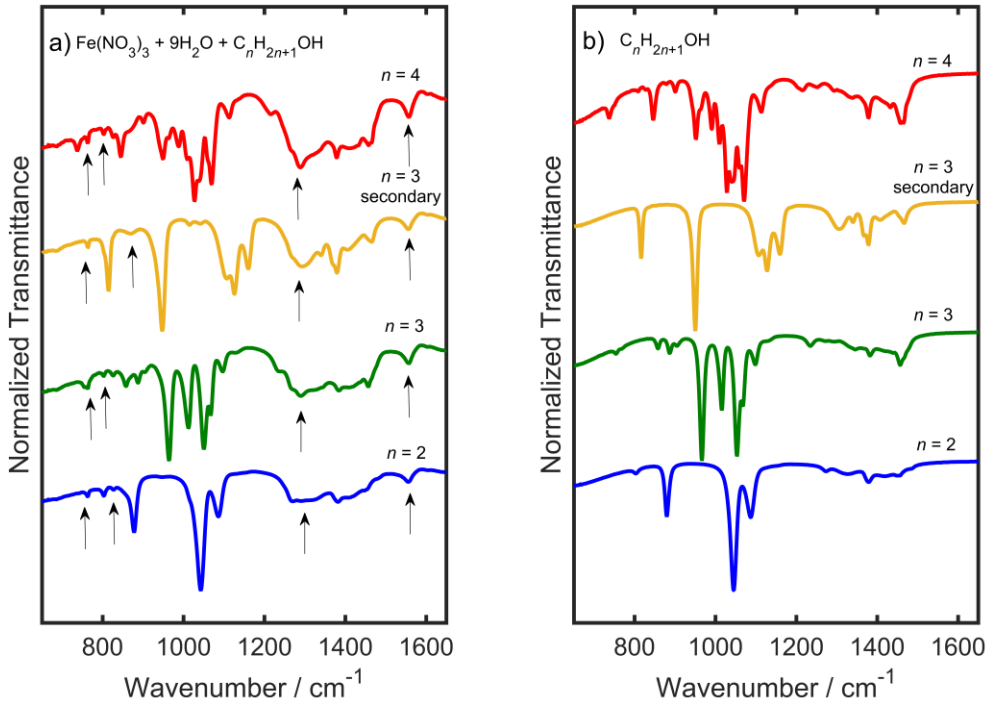

Figure 5: IR spectra of fingerprint region of dissolved iron(III) nitrate nonahydrate in *n*-alkyl alcohols with b = 1.0 mol kg^{-1} (a) and respective neat solvents (b).

As a consequence, the vibrational properties change, depending on increasing bond strength or decreasing bond strength. The width and shape of the band is owing to a number of different bonding states within the liquid. For the spectra of iron(III) nitrate nonahydrate in Figure 3, a sharp peak in the region of 3650 is revealing a fraction of non-hydrogen-bonded OH groups. This fraction is no longer visible in the IR spectra of the binary mixture in Figure 4 owing to effects of neighboring molecules and a strong reduction of not-hydrogen-bonded OH groups.

The CH stretching region is observed within the spectral range of 2700-3100 cm^{-1} and is, like the OH stretching mode, very characteristic for alkyl alcohols. Although only short chained alcohols with 2-4 methyl groups are screened within this work, distinct differences in the CH vibrations are observed, revealing a multitude of possible vibration modes. The IR bands in Figure 4 at 2800-3000 cm^{-1} can be assigned to symmetric and antisymmetric vibrations including in-plane and out-of-plane motions (Kiefer et al., 2018).

Figure 5a and b display the fingerprint region of the IR spectra recorded for dissolved iron(III) nitrate nonahydrate and neat solvents. This region is of special interest since molecular interactions between solvents and metals can be found here. While the molecular composition of alcohols does not change significantly with increasing chain length, there are quite significant differences in the vibrational spectra. This is due to a multitude of antisymmetric and symmetric bending/deformation and torsional and rocking modes of CH_2, CH_3, and OH groups (Kiefer et al., 2018; Plyler, 1952; Zheng et al., 2011). These bands are still observed at dissolving iron(III) nitrate nonahydrate in the solvents. However, the intensity increases systematically, as already shown in Figure 3 for ethanol as solvent, due to an overlap of NO_3 and OH vibrations from the nitrate and the dissolved water. Interestingly, new formed signatures are observed as indicated by arrows in Figure 5. These bands are rather weak and difficult to assign and seem to have origin in iron and solvent bonds and NO_3 stretching modes. The 1550 cm^{-1} band is of special interest as it is not consistent with literature data on NO_3 stretching and metalorganic vibration modes. The data suggest that there is a chemical reaction occurring forming a new compound, which is yet to be assigned.

Precipitation

Precipitation was observed for all investigated systems after at least 24 h for $b > 0.2$ mol kg^{-1} as a muddy, light brown turbidity at ambient conditions, as indicated in Figure 6. This chemical mechanism may occur with the oxidant iron(III) nitrate and alcohols in the presence of water from the nonahydrate. This water is released upon dissolution of the salt in the solvent and may give rise to the hydrolysis of iron(III) nitrate (Dressen et al., 2009):

$$2\ Fe(NO_3)_3 + 3\ H_2O \leftrightarrow Fe_2O_3 + 6\ HNO_3$$

This scheme also accords to the decreased pH value observed after dissolution of iron(III) nitrate in all solvents, caused by nitric acid. Nevertheless, the crystalline phase of the iron oxide is not fully identified yet. For further insights, the precipitated solid was filtered using a frit and then dried for 12 h at $T = 50$ °C in an oven at ambient pressure. IR measurements of the precipitated phase showed signatures of water and nitrate. Iron oxide was not observed since the characteristic bands of iron oxide can be found in the far infrared spectra at wavenumbers below 600 cm^{-1}.

Karlsruhe, Germany, ISBN 978-3-9816764-5-7

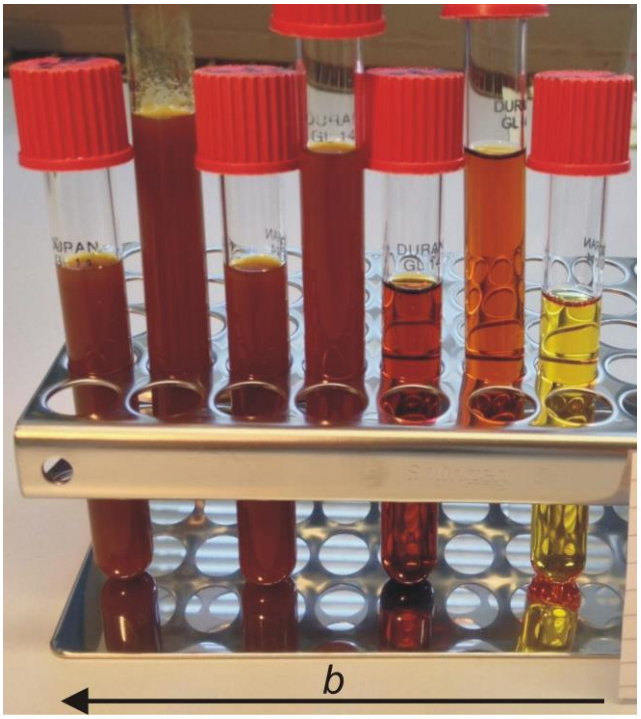

Figure 6: Samples of $Fe(NO_3)_3$ $9H_2O$ dissolved in 1-propanol after 24 h for a composition range of 0.01 mol kg^{-1} < b < 0.5 mol kg^{-1}.

Conclusions

IR spectroscopy has been employed to study the precursor chemistry of iron(III) nitrate nonahydrate and *n*-alkyl alcohols (*n* = 2, 3, 4) for a series of molalities in the range of 0.01 mol kg^{-1} < *b* < 1.0 mol kg^{-1}. A vibrational analysis is presented and a new formed vibrational band is detected, which is not fully understood yet and therefore subject of future research. Furthermore, significant precipitation was detected and a precipitation mechanism presented. Further X-ray experiments are necessary to investigate the exact composition and crystalline phase of the solid precipitated phase.
In conclusion, the precursor chemistry does have an effect on the fluid properties due to covalent interactions between iron and organic functional groups which may give rise to a multitude of molecular rearrangements and chemical reactions. Hence, different evaporation rates and droplet sizes can be expected during the FSP process. The atomization process and spray structure when using these precursors will be in focus in the next step of this investigation.

Acknowledgements

We acknowledge financial support from the Deutsche Forschungsgemeinschaft within the priority program SPP 1980 SPRAYSYN under Grants KI 1396/6-1 and FR 912/42-1.

Literature

Dressen, M. H., Stumpel, J. E., van de Kruijs, B. H., Meuldijk, J., Vekemans, J. A., & Hulshof, L. A. (2009). The mechanism of the oxidation of benzyl alcohol by iron (III) nitrate: conventional versus microwave heating. Green Chemistry, 11(1), 60-64.

Gröhn, A. J., Pratsinis, S. E., & Wegner, K. (2012). Fluid-particle dynamics during combustion spray aerosol synthesis of ZrO_2. Chem.Eng. J., 191, 491-502.

Kiefer, J., Wagenfeld, S., & Kerlé, D. (2018). Chain length effects on the vibrational structure and molecular interactions in the liquid normal alkyl alcohols. Spectrochimica Acta Part A: Molecular and Biomolecular Spectroscopy, 189, 57-65.

Mädler, L., Kammler, H., Mueller, R., & Pratsinis, S. E. (2002). Controlled synthesis of nanostructured particles by flame spray pyrolysis. J.of Aerosol Science, 33(2), 369-389.

Meierhofer, F., Li, H., Gockeln, M., Kun, R., Grieb, T., Rosenauer, A., . . . Mädler, L. (2017). Screening Precursor–Solvent Combinations for $Li_4Ti_5O_{12}$ Energy Storage Material Using Flame Spray Pyrolysis. ACS Applied Materials & Interfaces, 9(43), 37760-37777.

Mueller, R., Mädler, L., & Pratsinis, S. E. (2003). Nanoparticle synthesis at high production rates by flame spray pyrolysis. Chemical Engineering Science, 58(10), 1969-1976.

Paolantoni, M., Sassi, P., Morresi, A., & Cataliotti, R. S. (2005). Infrared study of 1-octanol liquid structure. Chemical physics, 310(1-3), 169-178.

Plyler, E. K. (1952). Infrared Spectra of Methanol, Ethanol, and rz-Propanol. J. of Research of the National Bureau of Standards, 48(4).

Sassi, P., Morresi, A., Paolantoni, M., & Cataliotti, R. S. (2002). Structural and dynamical investigations of 1-octanol: a spectroscopic study. J. of molecular liquids, 96, 363-377.

Wang, C.-s., Friedlander, S. K., & Mädler, L. (2005). Nanoparticle aerosol science and technology: an overview. China Particuology, 3(05), 243-254.

Zheng, R., Sun, Y., & Shi, Q. (2011). Theoretical study of the infrared and Raman line shapes of liquid methanol. Physical Chemistry Chemical Physics, 13(6), 2027-2035.